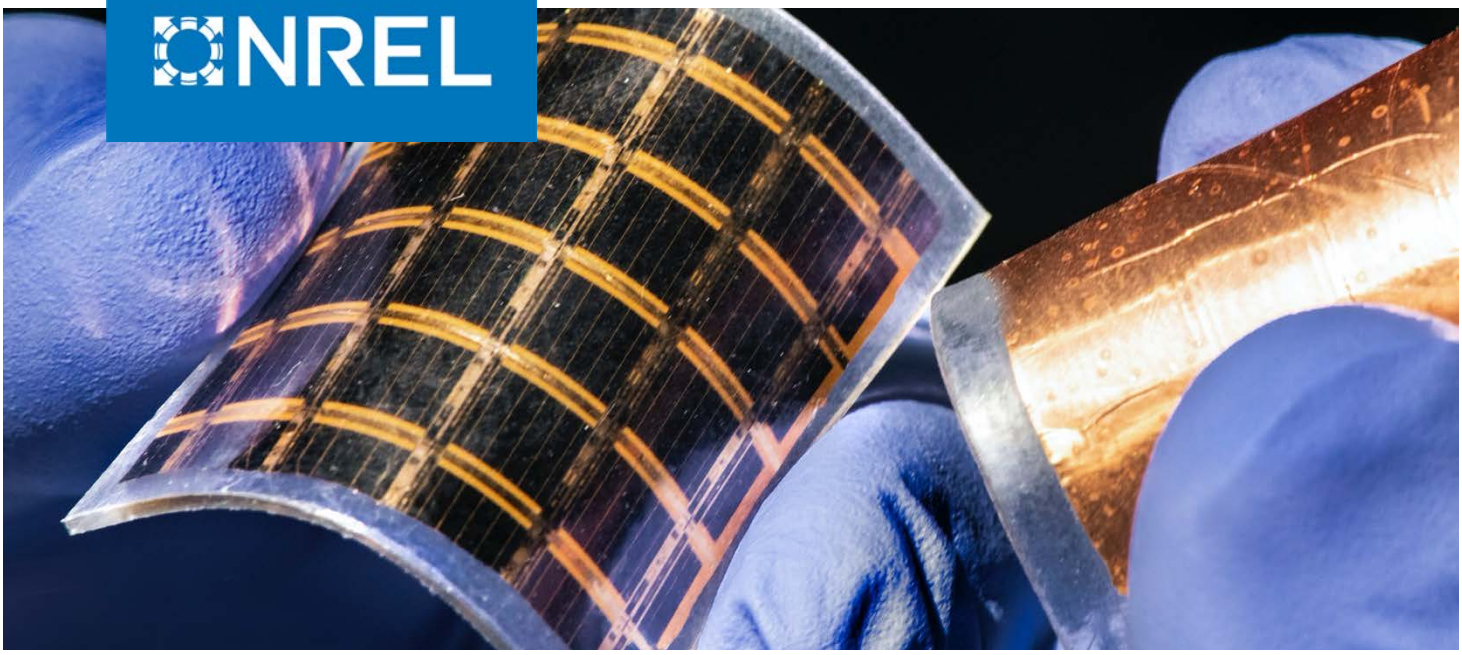

Radiation Effects in III-V Solar Cells Grown by Dynamic Hydride Vapor Phase Epitaxy

Aaron J. Ptak, Ryan M. France, and John Simon

National Renewable Energy Laboratory

NREL is a national laboratory of the U.S. Department of Energy
Office of Energy Efficiency & Renewable Energy
Operated by the Alliance for Sustainable Energy, LLC

This report is available at no cost from the National Renewable Energy Laboratory (NREL) at www.nrel.gov/publications.

Contract No. DE-AC36-08GO28308

Technical Report
NREL/TP-5900-79742
September 2021

Radiation Effects in III-V Solar Cells Grown by Dynamic Hydride Vapor Phase Epitaxy

Aaron J. Ptak, Ryan M. France, and John Simon

National Renewable Energy Laboratory

Suggested Citation
Ptak, Aaron J., Ryan M. France, and John Simon. 2021. *Radiation Effects in III-V Solar Cells Grown by Dynamic Hydride Vapor Phase Epitaxy*. Golden, CO: National Renewable Energy Laboratory. NREL/TP-5900-79742. https://www.nrel.gov/docs/fy21osti/79742.pdf.

NREL is a national laboratory of the U.S. Department of Energy
Office of Energy Efficiency & Renewable Energy
Operated by the Alliance for Sustainable Energy, LLC

This report is available at no cost from the National Renewable Energy Laboratory (NREL) at www.nrel.gov/publications.

Contract No. DE-AC36-08GO28308

Technical Report
NREL/TP-5900-79742
September 2021

National Renewable Energy Laboratory
15013 Denver West Parkway
Golden, CO 80401
303-275-3000 • www.nrel.gov

NOTICE

This work was authored by the National Renewable Energy Laboratory, operated by Alliance for Sustainable Energy, LLC, for the U.S. Department of Energy (DOE) under Contract No. DE-AC36-08GO28308. Funding provided by OSD OE-Innovation / Operational Energy Capability Improvement Fund. The views expressed herein do not necessarily represent the views of the DOE or the U.S. Government.

Executive Summary

The recent development of hydride vapor phase epitaxy (HVPE) is potentially promising as a route to lower the cost of high-efficiency III-V solar cells for space applications. HVPE produces the same materials and device structures as the industry-standard organometallic vapor phase epitaxy (OMVPE) process, and although HVPE has shown promising device efficiencies, it lags the OMVPE growth technique in technical maturity. For example, there are no reports of the performance of HVPE-grown devices in radiation environments. There is an expectation that high-quality (that is, single crystal and low-defect) III-V materials will behave similarly regardless of the growth method. However, it is important to verify assumptions as facts.

In this project, we produced materials and devices using both HVPE and OMVPE at NREL and irradiated them using 1 MeV electrons to ascertain the effect of radiation on the materials. We also performed initial work on producing more radiation-hard structures, including devices with the *p-n* junction at the front of the device, and devices with a graded doping profile, both of which help with radiation tolerance.

Measurements of the devices post radiation exposure showed that the open-circuit voltage (V_{OC}) of the HVPE-grown solar cells degraded least on a percent basis, although they also started from a lower baseline than the OMVPE-grown devices. All solar cells reached approximately the same V_{OC} after irradiation, indicating that the dose used was sufficient to degrade all devices equally. The short-circuit current in the HVPE devices did degrade more than the other solar cells, and this was attributed to a higher-than-expected doping density in the base layer of that cell.

The results of these experiments, while by no means comprehensive, do not show any material difference in the radiation effects in OMVPE- and HVPE-grown materials and devices.

Acknowledgements

We would like to thank the OSD OE-Innovation/Operational Energy Capability Improvement Fund for supporting this work. We are also very grateful to Yao Lao and Don Walker from The Aerospace Corporation for allowing us to piggyback on their radiation testing. We also thank Fred Bateman at NIST for performing the radiation exposures. In addition, we thank Waldo Olavarria, David Guiling, Michelle Young, and Evan Wong for materials growth and processing. We are also indebted to Dave Wilt at AFRL for substantial guidance and advice during this work. This work was authored by Alliance for Sustainable Energy, LLC, the manager and operator of the National Renewable Energy Laboratory for the U.S. Department of Energy (DOE) under Contract No. DE-AC36-08GO28308. This material is based upon work supported by the OSD OE-Innovation/Operational Energy Capability Improvement Fund. The views expressed in the article do not necessarily represent the views of the DOE or the U.S. Government. The U.S. Government retains and the publisher, by accepting the article for publication, acknowledges that the U.S. Government retains a nonexclusive, paid-up, irrevocable, worldwide license to publish or reproduce the published form of this work, or allow others to do so, for U.S. Government purposes.

Table of Contents

Table of Figures

Background

The production of 24% efficient (AM0) single-junction GaAs-based (III-V) solar cells and 28% efficient two-junction devices at costs below $30/W is a critical enabler for next-generation space power applications. Current solar technologies like silicon or cadmium telluride are not well-suited for space, and emerging technologies require significant research to understand their potential value in these demanding environments. Solar cells based on GaAs, however, have the highest light-to-electricity conversion efficiency, with single-junction devices achieving 29.1% under 1-sun (terrestrial) illumination [1]. Additionally, these devices have the highest power-to-mass ratio (W/kg) and lowest temperature coefficient [2] of any cell technology, making them ideal for light-weight, high-power applications that maintain their efficiency advantage in extreme, high- and low-temperature conditions. Importantly, III-V cells have a proven track record of reliability in very demanding space applications. Currently, however, these thin, stable, light, and flexible solar cells cost between $150 - $200/W, making them prohibitively expensive for use in large-area, high-power solar arrays. Solar cell costs today can be in excess of 50% of the entire cost of a large orbital installation. Drastically decreasing the cost of high-efficiency III-V solar cells can enable projects that are currently not feasible.

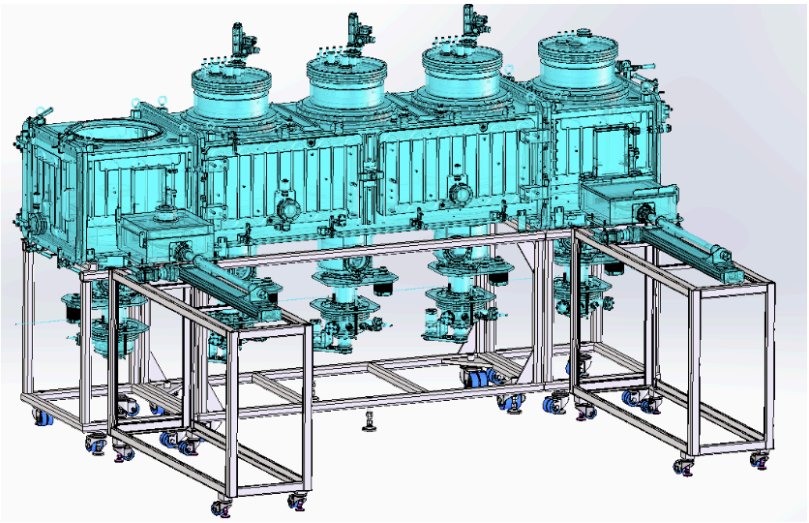

Figure 1. Schematic representation of the D-HVPE reactor under construction.

There are three major costs associated with the production of GaAs-based solar cells, each of which needs to be reduced before widespread adoption in large-area space applications can occur: the costs associated with epitaxial growth, substrate reuse, and back-end processing. Scaling the overall manufacturing process also plays a critical role in achievable costs.

New manufacturing platform for low-cost epitaxial growth: Hydride vapor-phase epitaxy (HVPE) is a well-established route to grow very high-quality semiconductors. Compared with organometallic vapor phase epitaxy (OMVPE) growth, HVPE has > 10x higher deposition rate, uses input materials that are 10x less expensive, has a much higher material utilization rate, and lends itself to a low-cost, in-line deposition process [3]. All together these features make HVPE a low-cost manufacturing technique. HVPE is currently used in the batch manufacturing of *substrates* for LEDs and power electronics devices, but has not been used to produce *devices* themselves due to difficulties in growing clean and abrupt interfaces–until now.

NREL developed a pseudo in-line prototype *Dynamic*-HVPE (D-HVPE) growth reactor for GaAs-based *devices* that solves the interface growth problem by rapidly moving the substrate between different growth chambers separated by gas curtains. D-HVPE research showed, for the first time, **>25% efficient AM1.5G GaAs solar cells grown ~ 30x faster** than OMVPE [4]. NREL also demonstrated the world's first HVPE-grown two-junction devices with a direct path to > 28% AM0 efficiency. Currently, NREL is engaged in designing and building a three-chamber, pseudo in-line D-HVPE reactor with the capability to deposit on industry-standard 6" wafers, shown in Figure 1. This new system, once delivered, will dramatically increase the throughput of III-V solar devices through significantly higher growth rates and the use of the pseudo in-line process.

Lower costs are not always valuable, however, if the materials and devices do not perform equivalently to existing products. The space environment subjects solar cells to high levels of electron and proton radiation, depending on the orbit, that create point defects within the materials. These defects adversely affect the performance of the devices, leading to decreasing conversion efficiencies throughout the mission. Fortunately, the degradation mechanisms are well-understood and fairly predictable as a function of radiation fluence and energy. Irradiation using controlled conditions in a terrestrial setting is often used to determine degradation rates for different materials and device structures. It is important to quantify the degradation of solar cells grown by the new D-HVPE method to understand if they will perform equally well as current devices in the relevant space environments. It is likely that all III-V materials, regardless of growth method, will perform similarly, *i.e.,* "GaAs is GaAs." However, it is also possible that a specific growth method may lead to a difference in the original point defect types or concentrations that lead to different overall behavior upon irradiation.

Objectives

There are three main objectives in this work:

1. Development of front-junction device structures using D-HVPE
2. Development of graded base doping using both D-HVPE and OMVPE
3. Assessment of solar cell performance after irradiation and post-irradiation recovery

Development of front-junction device structures using D-HVPE

Growth of device structures using our current, custom, two-chamber D-HVPE system at NREL, shown in Figure 2, involves depositing a layer on a substrate in one growth chamber while establishing growth conditions for a subsequent layer in the adjacent chamber. The substrate then moves to the adjacent chamber for growth of that specific device layer in a process known as *dynamic* HVPE, and the procedure continues until the entire device structure is complete. This substrate motion is in contrast to the standard OMVPE growth method that switches gases and relies on plug flow to create abrupt interfaces between layers and is necessary in HVPE growth due to high growth rates and significant chemical inertia during the growth process, which is described in more detail elsewhere [5, 6]. For the purposes of this study, the D-HVPE process used here results in layers of a specific material, alloy composition, doping, or growth rate being calibrated in a specific growth chamber, and each layer being somewhat dependent on the order in which layers are deposited, again in contrast to OMVPE growth. Any device structure can be obtained using D-HVPE, but the practical ramifications of this approach are that a change in structure requires recalibration of the entire layer stack.

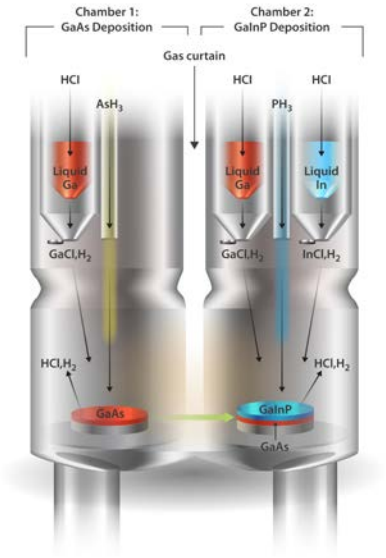

Figure 2. Schematic representation of the current, custom D-HVPE reactor in use at NREL.

Before this project, most GaAs solar cells grown by D-HVPE used a rear heterojunction (RHJ) structure that is more appropriate for terrestrial applications. The RHJ structure, shown schematically in Figure 3 (left), results in a slightly higher efficiency due to lowered depletion region recombination at the buried heterointerface [7, 8]. However, this structure depends on the diffusion of minority-carrier holes and requires very high material quality. The literature shows that structures with deep junctions do not fare well in space environments once radiation-induced degradation begins, as shown in Figure 4 [9]. Therefore, we developed the front junction structure, also shown in Figure 3 (right), by D-HVPE as a part of this project to improve radiation resistance.

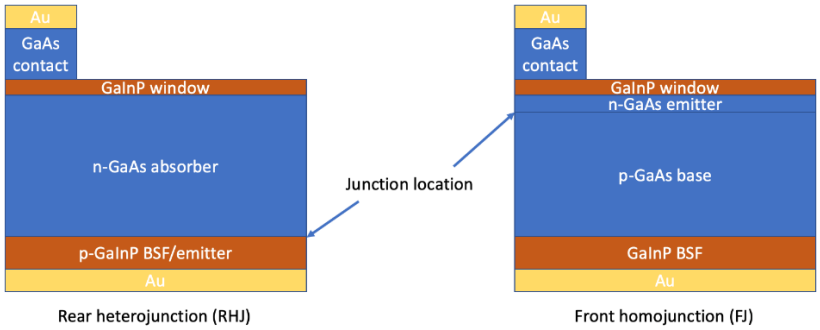

Figure 3. Front and rear junction solar cell structures.

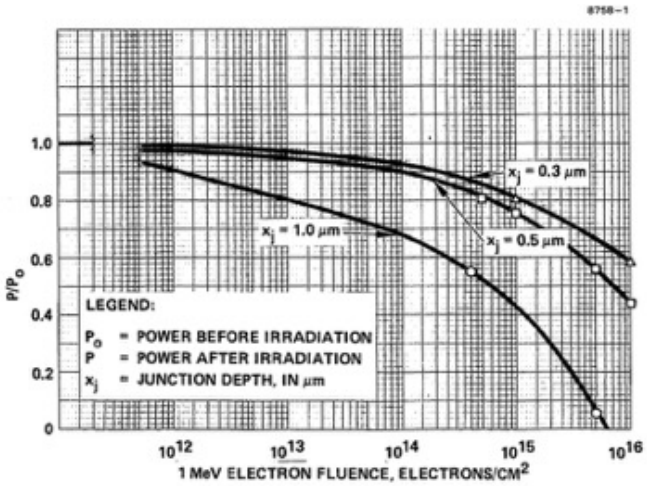

Figure 4. Comparison of the performance of irradiated solar cells as a function of junction depth showing that front junction structures maintain higher performance compared to rear junctions. From [9].

Development of graded base doping using both D-HVPE and OMVPE

Another structural change that improves radiation resistance is the incorporation of graded doping in the solar cell absorber layer, shown schematically in Figure 5. This grade creates an electric field within the device that helps to "sweep" minority carriers toward the junction. Typically, carriers diffuse to the junction, but this process relies on high material quality and long minority-carrier diffusion lengths, which are controlled in large part by point defects. Radiation increases the point defect concentration in the solar cell and decreases the diffusion length. Once the average diffusion length is less than the distance the carriers need to travel for collection, performance suffers. The electric drift field works as a boost to the diffusion process and continues to allow for carrier collection when the diffusion length decreases.

Graded layers are what D-HVPE was specifically designed to avoid, and despite decades of research on OMVPE growth of solar cells at NREL, there was little experience creating these doping profiles. Therefore, this project aimed to develop graded doping in front-junction solar cells by both OMVPE and D-HVPE.

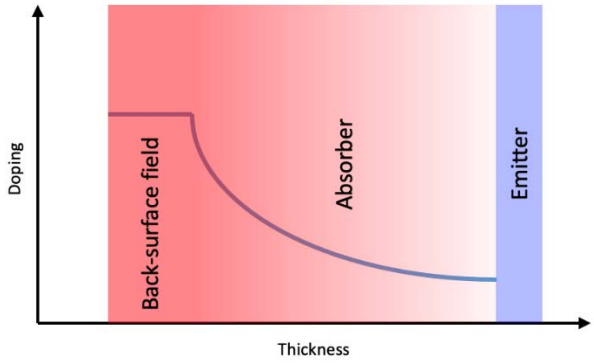

Figure 5. Schematic showing the carrier doping profile that creates an electric field within the device that helps carrier collection when diffusion lengths decrease due to radiation damage.

Assessment of solar cell performance after irradiation and post-irradiation recovery

This was the main objective of this project. There was an expectation that GaAs solar cells with similar terrestrial performance would perform similarly under space conditions regardless of how they were created. However, it is important to positively establish that this is the case. We deposited GaAs solar cells by both OMVPE and D-HVPE with as close to the same structure as possible and irradiated them with high-energy electrons to show how each degraded. We also performed post-irradiation annealing and light soaking to show how each responded. The results from these experiments are detailed below.

Results and Analysis

Development of front-junction device structures using D-HVPE

As discussed above, growth of a front-junction structure by D-HVPE, like the one shown in Figure 3, required re-optimization of each of the device layers. This took time but did not present any serious technical challenges. Figure 6 shows the current-density-voltage (*JV*) measurement of a front-junction GaAs solar cell grown by D-HVPE. The measurement used AM0 illumination conditions and resulted in an open-circuit voltage (V_{OC}) of ~ 1.03 V and a conversion efficiency of ~ 20%.

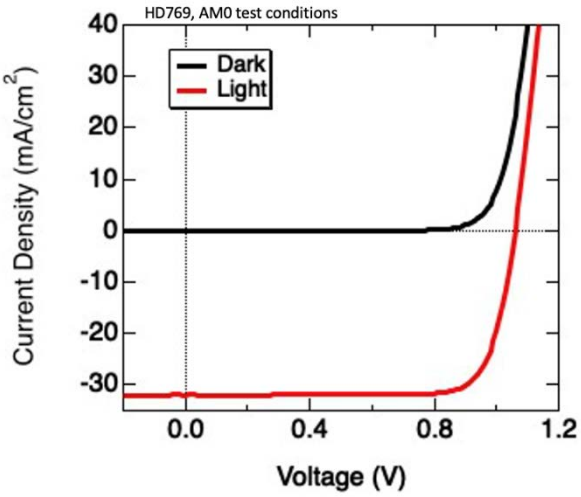

Figure 6. Current-density-voltage (JV) measurement of a front-junction GaAs solar cell grown using D-HVPE under AM0 (space) illumination conditions. The efficiency was ~ 20%.

Development of graded base doping using both D-HVPE and OMVPE

Doping with Zn in the D-HVPE systems is complicated by the fact that there is ~ 10 m of ¼" stainless steel line between the Zn source (a diethylzinc bubbler) and the growth reactor. It takes a significant amount of time (several minutes, at least, depending on the total flow in the line) to prime these lines with Zn, and an equal amount of time for any changes in the Zn flow to reach the growth surface. This makes the deposition of a layer with a controlled graded doping profile difficult to achieve in practice. The growth rates in HVPE are typically very high, minimally on the order of 1 µm/min. Thus, a 2-µm-thick base layer is finished before meaningful changes to the Zn flow can be made.

We were able to achieve some level of Zn profile control by changing the Zn flow well before it was needed for the base layer growth. Figure 7 shows a secondary ion mass spectrometry (SIMS) measurement of the Zn concentration in a D-HVPE-grown GaAs solar cell, with the Zn concentration rising toward the back of the device and creating an electric field that aids carrier drift. This profile is not optimal, but it did achieve a conversion efficiency on par with a similar solar cell grown with constant doping. Figure 8 shows a comparison of the *JV* curves for these devices, measured under the AM1.5G terrestrial spectrum. They are expected to be ~ 20% efficient under AM0 space conditions.

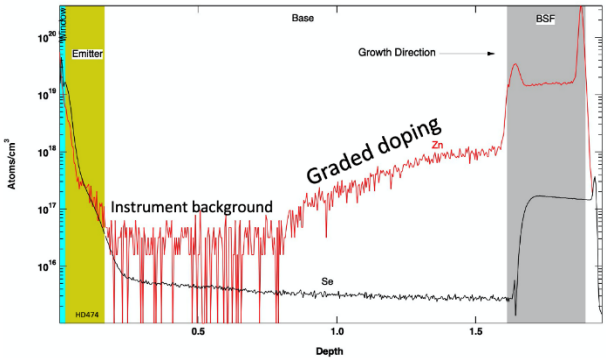

Figure 7. Secondary-ion mass spectrometry (SIMS) measurement showing the Zn and Se concentrations as a function of depth in a solar cell grown using D-HVPE. The Zn profile shows graded doping.

Graded doping development was more straightforward by OMVPE. We performed calibrations to determine the Zn concentration resultant in GaAs as a function of Zn mass flow controller settings, then used these data to design an exponential doping profile. Figure 9 shows measurements of the acceptor doping from capacitance-voltage measurements, the Zn concentration from SIMS measurements, and the designed doping profile. There is reasonable agreement between the data. Figure 10 shows a comparison of solar cells grown by OMVPE with either a flat doping profile or the profile shown in Figure 9. The performance of the two devices is nearly identical, with AM0 space performance of ~ 21.5% conversion efficiency.

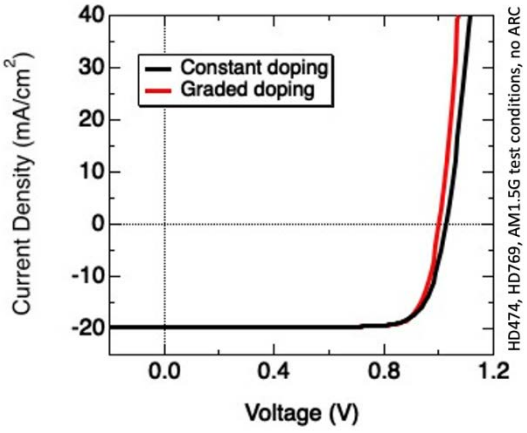

Figure 8. JV curves comparing the performance of two D-HVPE-grown GaAs solar cells, with graded or constant Zn doping in the base layer.

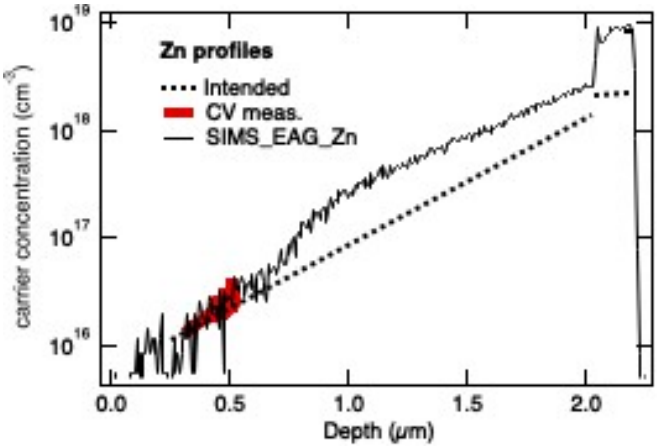

Figure 9. Comparison of Zn doping determined by capacitance-voltage (CV) and SIMS measurements, along with the intended profile.

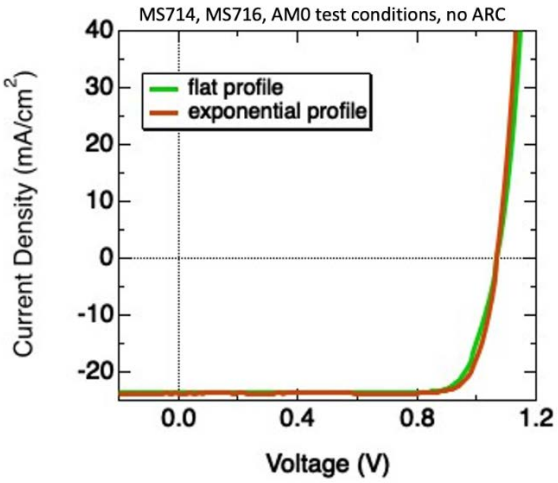

Figure 10. Comparison of OMVPE-grown GaAs solar cell JV curves for devices with flat or exponential doping. The devices each have conversion efficiencies of ~ 21.5% under AM0 conditions.

Assessment of solar cell performance after irradiation and post-irradiation recovery

We produced two different structures for testing with high-energy radiation. The first was a front junction (FJ) solar cell structure like those shown in the right side of Figure 3. The FJ structures allow for measurement of the full *JV* curve before and after irradiation, as well as the doping of the base through capacitance techniques. As shown above, graded doping by HVPE was problematic so only flat doping samples were produced by HVPE for this study. We were able to measure both flat and exponentially-doped devices grown by OMVPE. The doping of the HVPE-grown device was higher than intended, ~ 5 x 10^{17} cm^{-3} instead of 1 x 10^{17} cm^{-3}. This likely decreased the minority-carrier lifetime and diffusion length in these devices, in part contributing to the lower performance compared to the OMVPE-grown cells. However, we do not expect that this difference materially alters the conclusions of this study. We grew these cells with relatively thick base layers, measured in each cell to be ~ 1.9 μm, to better observe degradation in the short-circuit current density (J_{SC}).

The second structures that we produced were double heterostructures (DHs), which are "sandwiches" of a material of interest, in this case GaAs, clad on the front and back surfaces with a higher bandgap material, here GaInP. The DH structures allow for the measurement of the minority-carrier lifetime by using time-resolved photoluminescence (TRPL). This measurement involves illuminating a sample with a very fast laser pulse and recording the intensity of the resultant luminescence as a function of time. This leads to an estimate of the minority-carrier lifetime, that is, the longer the photoluminescence persists, the longer the carrier lifetime, although this analysis can be complicated by carrier trapping. Our measurements used a 670 nm laser with a

1 MHz duty cycle. Typically, TRPL measurements use samples of varying thickness to extract the interface recombination velocity and the bulk minority-carrier lifetime, according to:

$$\frac{1}{\tau_{TRPL}} = \frac{1}{\tau_{bulk}} + \frac{2S}{d} \qquad (1)$$

where τ_{bulk} is the minority carrier lifetime of the material of interest, S is the interface recombination velocity, and d is the thickness of the layer. All structures were irradiated at the National institute of Standards and Technology using 1 MeV electrons and different total fluences, as described below, and as shown in Table II in Appendix A. The structures were measured before and after irradiation, then were subjected to additional post-irradiation recovery efforts. The first was a 24 h anneal at 60°C in the dark, and the second was a 48 h light soak using AM0 illumination at 28°C. Structures were also measured after each of these steps.

Figure 11 shows the TRPL lifetimes measured from HVPE- and OMVPE-grown GaAs DHs with different GaAs thicknesses. There is a difference in the lifetimes between the two sets prior to irradiation, with OMVPE samples having typical lifetimes near 9 nsec, compared to ~ 3 nsec for HVPE samples. Again, this is likely due to the higher base doping in the HVPE-grown structures. For reference, the radiative lifetimes for GaAs doped at either 1 or 5 x 10^{17} cm^{-3} are ~ 50 nsec and 10 nsec, respectively. We attempted to extract values for S and τ_{bulk} but there was enough scatter in the data to make the fits unreliable. From the flatness of the trends, we can infer that the recombination velocity is below 1000 cm/s and unlikely to be a limiting factor in solar cells grown using these conditions. Upon irradiation with a fluence of 1 x 10^{15} cm^{-2} 1 MeV electrons, all samples, regardless of growth method, had lifetimes of 0.2 – 0.3 nsec. We irradiated other DH structures with other fluences of electrons but did not have the resources necessary to complete the measurements and analysis.

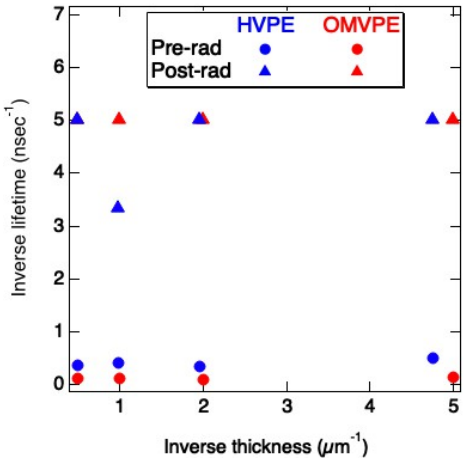

Figure 11. TRPL lifetime measurements comparing HVPE- and OMVPE-grown GaAs DH structures.

We also irradiated the FJ solar cells with 1 x 10^{15} cm^{-2} 1 MeV electrons. Figure 12 shows results of the pre- and post-irradiation measurements. The plots in the left column show the pre-irradiation *JV* curves in black. Note that none of these devices had an anti-reflection coating applied. The red data in each case is the *JV* measurement taken directly after 1 MeV electron irradiation. The green and blue data are the measurements after the dark anneal and light soak conditions described above, respectively. The plots in the right column are the same data, but magnified in the region around V_{OC}. Clearly, the 1 MeV electron irradiation caused significant degradation in each case in both the V_{OC} and the J_{SC}. Figure 13 shows the V_{OC}, J_{SC}, fill factor (FF) and efficiency determined from the data in Figure 12 for each of the measurement conditions. Figure 14 shows the same data, normalized to unity.

It is clear from the normalized data shown in Figure 14 that the HVPE-grown solar cell had the lowest percent change in V_{OC} of any of the devices measured. However, this device also started with the lowest V_{OC} and can hence be considered "pre-degraded" in some sense. As discussed above, this beginning of life (BOL) degradation is most likely due to the high base doping, and hence lower lifetime, in these devices compared to the OMVPE growths. After irradiation with a fluence of 1 x 10^{15} cm^{-2} 1 MeV electrons, all the devices showed essentially identical V_{OC}. This likely means that if the HVPE-grown device had started with a higher V_{OC}, that it too would have had a relatively larger percent change and ended up at the same level as the OMVPE-grown solar cells. This seems to indicate that even though the devices started with different performance levels, this fluence of 1 MeV electrons was sufficient to degrade them all to the same final state.

The degradation in the J_{SC} for the HVPE-grown cells, however, is quite a bit larger than for the OMVPE-grown devices. This is the primary reason that the irradiated efficiency of the HVPE solar cells is the lowest of the set, rather than serious degradation of the V_{OC}. It is possible that the higher-than-expected doping in the HVPE-grown device is responsible for this effect. The high doping will lead to a shorter minority-carrier diffusion length in the as-grown material. Upon irradiation, it is possible that this diffusion length becomes short enough to significantly affect the carrier collection, especially in the absence of an electric field arising from a built-in graded doping profile. We note that the J_{SC} of the OMVPE-grown solar cell with the exponential doping fared quite well, and that while there was degradation in the flat-doped version, it may not have been as severe as the HVPE cell due to the lower original base doping. To test this, we modelled the internal quantum efficiency (IQE) for each of the solar cells using data generated before and after irradiation. Figure 15 shows the modeled fits for the HVPE-grown device. We performed similar modeling for the OMVPE devices. It is difficult to get an accurate fit when the minority-carrier diffusion length is significantly longer than the thickness of the base layer. In this case we can only estimate that it is larger than some minimum value. In the case of this modeling effort, we estimate that both the OMVPE and HVPE solar cells had diffusion lengths > 5 μm before irradiation. After irradiation, both devices showed similar degradation, as shown in Table I. Because of the square root dependence of the diffusion length on the minority-carrier lifetime, these data also agree with the TRPL data. There was an order of magnitude decrease (or more) in the decay lifetime upon irradiation, which would lead to a decrease in the diffusion length of three to four times, which is approximately what we see here.

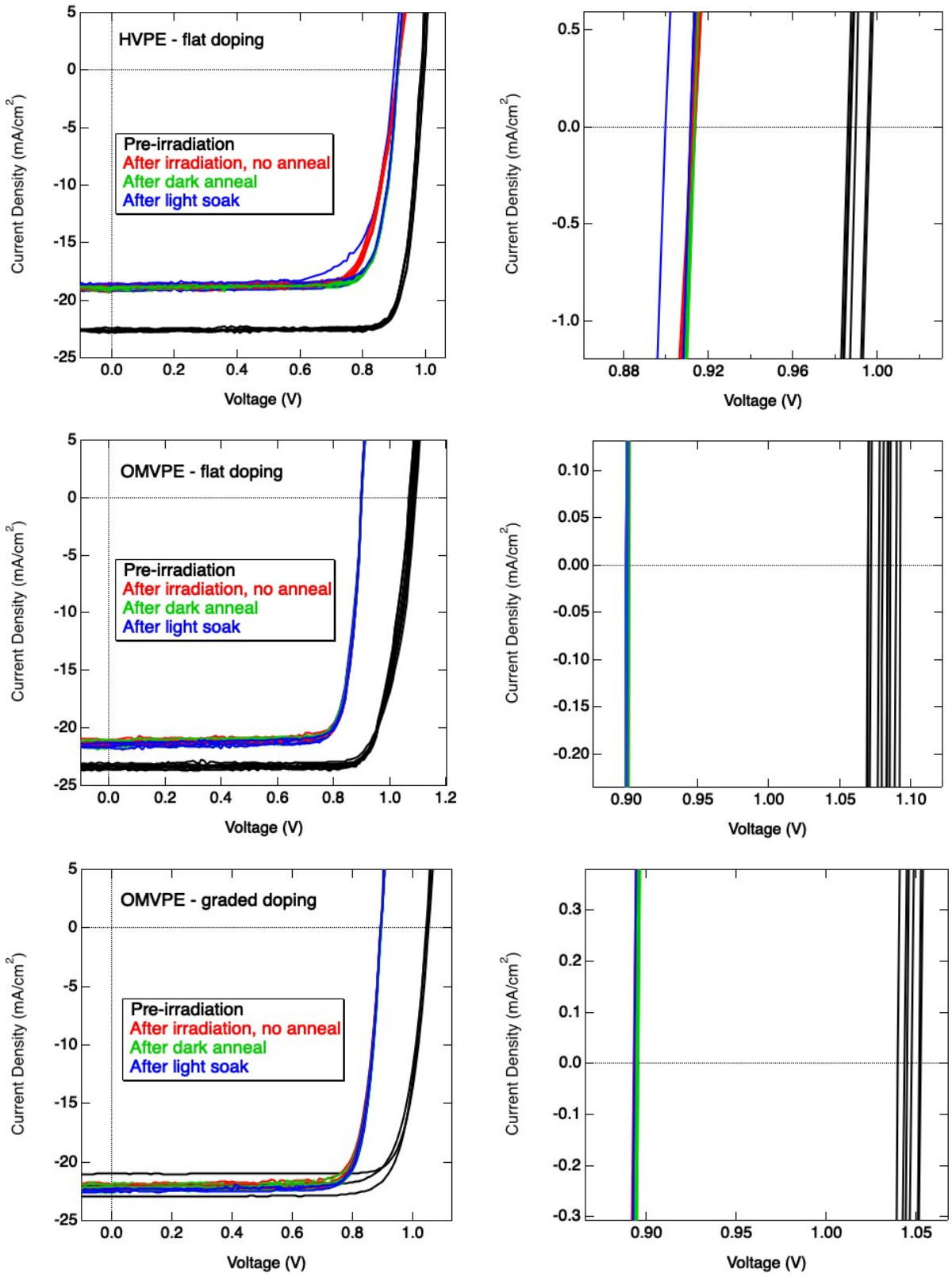

Figure 12. Pre- and post-irradiation JV curves for the solar cell structures tested here. The right column shows the same data as on the left, magnified near the open-circuit voltage.

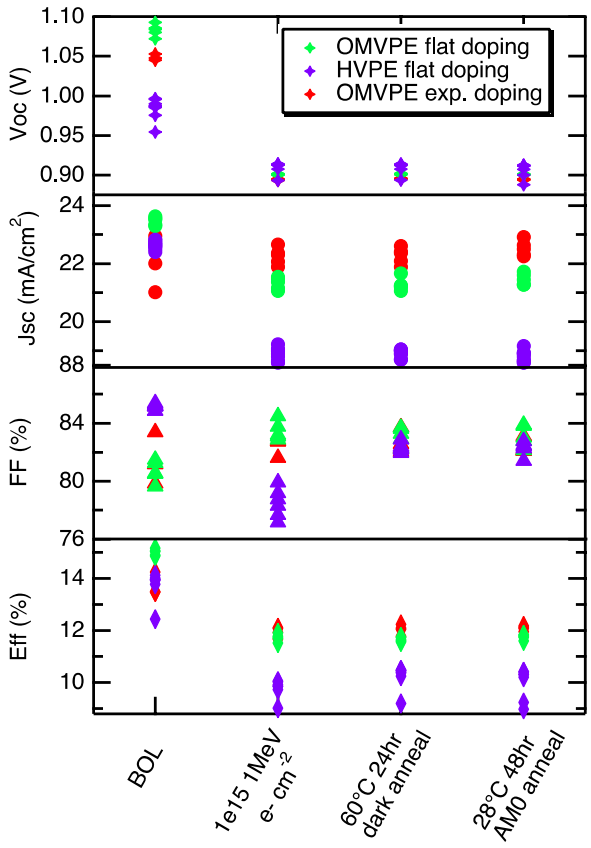

Figure 13. Solar cell parameters measured from the JV curves shown in Figure 12.

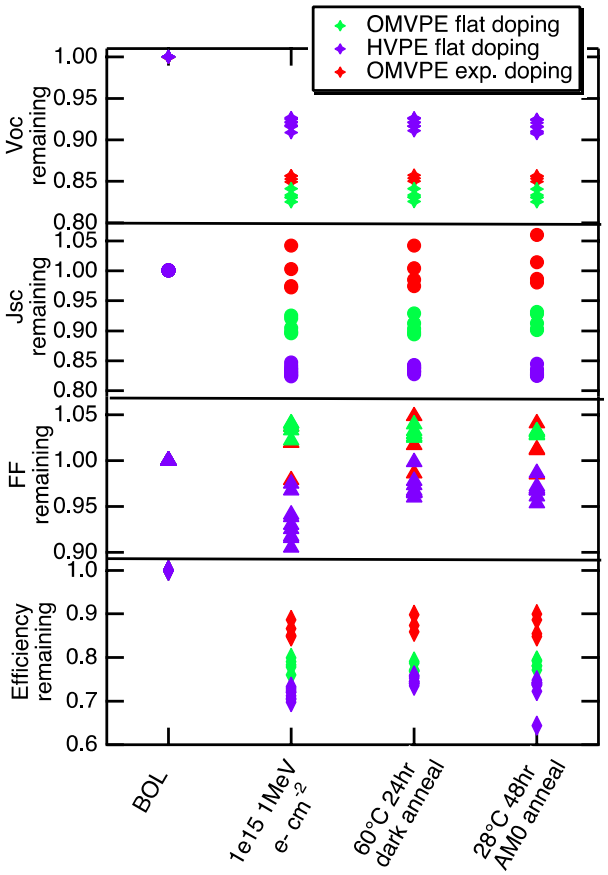

Figure 14. Solar cell parameters shown in Figure 13, normalized to unity.

We believe that the OMVPE-grown device had a higher diffusion length than the HVPE sample before irradiation because of its lower base doping. Measurements showed that none of the base doping levels changed throughout these experiments. Other structural changes, in addition to attaining a proper doping profile, can help with J_{SC} retention as well, including thinner base layers and the use of a metallic back reflector or distributed Bragg reflector.

We performed the dark annealing and light soaking experiments that form part of the qualification standards set forth by the U.S. and European communities. Clearly, the experiments performed here are nowhere near as rigorous as required for full qualification but are intended to provide initial information of the degradation of HVPE-grown materials and devices. The additional processing resulted in minor improvements in the J_{SC} for some devices, and the FF of the HVPE solar cells, but little else of note.

Table I. Estimated diffusion lengths from the IQE fitting shown in Figure 15.

	HVPE	OMVPE
Pre-rad	> 5 μm	> 5 μm
Post-rad	1.6 μm	2.3 μm

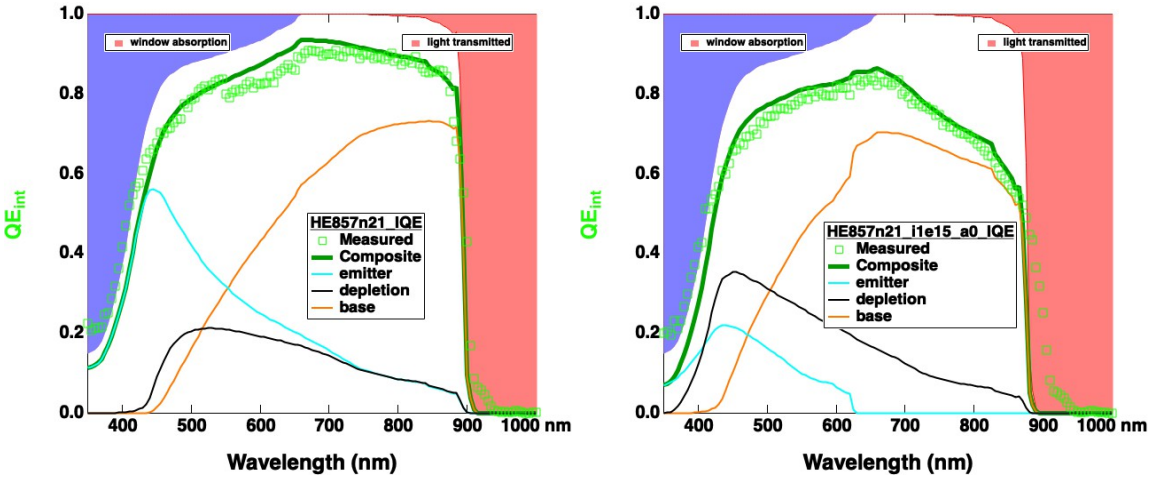

Figure 15. Modeling of the IQE for the HVPE-grown solar cell for both before (left) and after (right) irradiation.

We noted an interesting effect during TRPL measurements. Figure 16 shows carrier lifetimes extracted from TRPL measurements for both HVPE- and OMVPE-grown DHs. These measurements occurred after irradiation. These data show that the lifetime increases as a function of time during the TRPL measurements. The laser light incident on the samples creates a healing effect that reduces some of the radiation degradation. Thinner samples heal more than thicker samples, likely due to the limited penetration depth of the laser light. Previous studies showed healing due to light soaking, but it is unclear if this laser-induced healing is a novel effect. The healing occurred when using a photon fluence of 1 x 10^{18} cm^{-3} but did not occur for a fluence of 1 x 10^{16} cm^{-3}. We estimate that the power of the higher fluence corresponds to a 30x concentration level, albeit at a single wavelength. We did not test the long-term stability of the healing effect and can only say that it was stable over the several minutes required to do the measurements. Both the long-term stability and the underlying physical mechanism warrant additional investigation. Figure 16 again shows that regardless of growth method, at t = 0 essentially all the samples have the same minority-carrier lifetime, similar to Figure 11, and that at the end of the experiment all of the samples again have roughly the same lifetime. It is likely that the DH structures heal much more than the solar cells due to the much higher illumination intensity during these laser-based measurements.

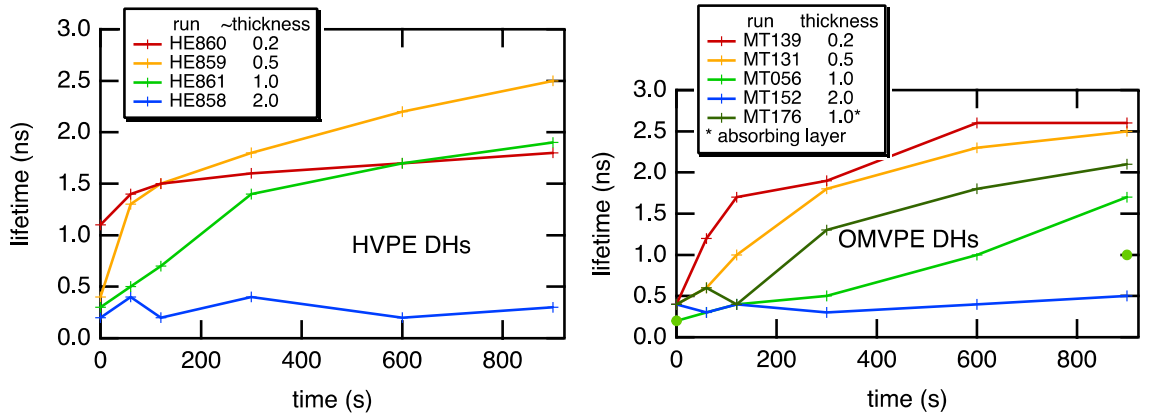

Figure 16. Minority-carrier lifetimes calculated from time-resolved photoluminescence measurements of irradiated DH structures as a function of laser illumination time.

Conclusions

In this project we developed front-junction GaAs solar cell structures using HVPE and preliminary graded doping profiles in solar cells grown by both HVPE and OMVPE. These were necessary steps toward hardening the cells to radiation effects. The graded doping in HVPE was complicated by the very long supply lines for the diethylzinc dopant source. We expect that moving the sources closer or other engineering-level changes will alleviate this issue in the future.

We irradiated both solar cells and double heterostructures grown by HVPE and OMVPE using 1 MeV electrons. Solar cells receiving a fluence of 1 x 10^{15} cm^{-2} electrons all had approximately the same V_{OC} regardless of the growth method used. The major difference between the irradiated solar cells was a larger decrease in the J_{SC} of the HVPE-grown devices. We speculated that this could be due to a higher doping level than optimal for this structure.

The purpose of this study was to determine if materials and devices grown using HVPE showed materially different behavior upon irradiation. The work here is preliminary and falls far short of the standards for space qualification. However, there is no indication in the collected data that suggests that HVPE-grown devices will degrade any differently than those currently produced for space applications.

References

[1] M. Green, E. Dunlop, J. Hohl-Ebinger, M. Yoshita, N. Kopidakis, and X. Hao, "Solar cell efficiency tables (version 57)," *Progress in Photovoltaics: Research and Applications,* vol. 29, no. 1, pp. 3-15, 2021, doi: https://doi.org/10.1002/pip.3371.

[2] T. J. Silverman, M. G. Deceglie, B. Marion, S. Cowley, B. Kayes, and S. Kurtz, "Outdoor performance of a thin-film gallium-arsenide photovoltaic module," presented at the Photovoltaic Specialists Conference (PVSC), 2013 IEEE 39th, 16-21 June 2013, 2013.

[3] K. Schulte *et al.*, "Computational fluid dynamics-aided analysis of a hydride vapor phase epitaxy reactor," *Journal of Crystal Growth,* vol. 434, pp. 138-147, 2016.

[4] J. Simon, K. L. Schulte, K. Horowitz, T. Remo, D. L. Young, and A. J. Ptak, "Enabling a renaissance in III-V-based optoelectronics with low-cost dynamic hydride vapor phase epitaxy," *Submitted,* 2018.

[5] J. Simon, K. L. Schulte, K. A. W. Horowitz, T. Remo, D. L. Young, and A. J. Ptak, "III-V-Based Optoelectronics with Low-Cost Dynamic Hydride Vapor Phase Epitaxy," *Crystals,* vol. 9, no. 1, p. 3, 2018. [Online]. Available: http://www.mdpi.com/2073-4352/9/1/3.

[6] K. L. Schulte, A. Braun, J. Simon, and A. J. Ptak, "High growth rate hydride vapor phase epitaxy at low temperature through use of uncracked hydrides," *Applied Physics Letters,* vol. 112, no. 4, p. 042101, 2018, doi: 10.1063/1.5013136.

[7] J. F. Geisz, M. A. Steiner, I. García, R. M. France, D. J. Friedman, and S. R. Kurtz, "Implications of Redesigned, High-Radiative-Efficiency GaInP Junctions on III-V Multijunction Concentrator Solar Cells," *IEEE Journal of Photovoltaics,* vol. 5, no. 1, pp. 418-424, 2015, doi: 10.1109/JPHOTOV.2014.2361014.

[8] Y. Sun, A. Perna, and P. Bermel, "Comparing Front- and Rear-Junction GaInP Photovoltaic Devices Through Detailed Numerical and Analytical Modeling," *IEEE Journal of Photovoltaics,* vol. 9, no. 2, pp. 437-445, 2019, doi: 10.1109/JPHOTOV.2019.2892530.

[9] S. Kamath, R. C. Knechtli, R. Loo, and B. E. Anspaugh, "Fabrication of high efficiency and radiation resistant GaAs solar cells," presented at the NASA. Lewis Res. Center Solar Cell High Efficiency and Radiation Damage, 1979, 1979, 1979.

Appendix A

Table II. Sample descriptions and measurement conditions for all irradiated samples.

HVPE Samples	Structure	Size (mm x mm)	Fluence (cm^{-2})
HE858A	DH	10x10	1.00E+14
HE859A	DH	10x10	1.00E+14
HE860A	DH	10x10	1.00E+14
HE861A	DH	10x10	1.00E+14
HE858B	DH	10x10	5.00E+14
HE859B	DH	10x10	5.00E+14
HE860B	DH	10x10	5.00E+14
HE861B	DH	10x10	5.00E+14
HE858C	DH	10x10	1.00E+15
HE859C	DH	10x10	1.00E+15
HE860C	DH	10x10	1.00E+15
HE861C	DH	10x10	1.00E+15
HE858D	DH	10x10	3.00E+15
HE859D	DH	10x10	3.00E+15
HE860D	DH	10x10	3.00E+15
HE861D	DH	10x10	3.00E+15
HE857	FJ Cell	25x25	1.00E+15
OMVPE samples	**Structure**	**Size (mm x mm)**	**Fluence**
MS845A	FJ Cell	15x20	1.00E+15
MT130A	FJ Cell	15x20	1.00E+15
MT302A	FJ Cell	15x20	1.00E+15
MT131C1	DH	4x8	1.00E+14
MT131C2	DH	6x10	5.00E+14
MT131C3	DH	6x10	1.00E+15
MT131C4	DH	4x10	3.00E+15

MT139C1	DH	4x8	1.00E+14
MT139C2	DH	6x10	5.00E+14
MT139C3	DH	6x10	1.00E+15
MT139C4	DH	4x10	3.00E+15
MT027C1	DH	4x4	1.00E+15
MT027C2	DH	5x10	1.00E+15
MT027C3	DH	5x10	1.00E+15
MT027C4	DH	5x10	1.00E+15
MT056C2	DH	5x10	5.00E+14
MT056C3	DH	5x10	1.00E+15
MT176C1	DH	4x8	1.00E+14
MT176C2	DH	6x10	5.00E+14
MT176C3	DH	6x10	1.00E+15
MT176C4	DH	4x10	3.00E+15
MT152C1	DH	5x10	1.00E+14
MT152C2	DH	6x10	5.00E+14
MT152C3	DH	6x10	1.00E+15
MT152C4	DH	5x10	3.00E+15
MT082C1	DH	5x5	1.00E+14
MT082C2	DH	6x10	5.00E+14
MT082C3	DH	6x10	1.00E+15
MT082C4	DH	5x10	3.00E+15
MT065C1	DH	4x8	1.00E+14
MT065C2	DH	6x10	5.00E+14
MT065C3	DH	6x10	1.00E+15
MT065C4	DH	4x10	3.00E+15
MT018C1	DH	5x5	1.00E+14
MT018C2	DH	6x10	5.00E+14
MT018C3	DH	6x10	1.00E+15

MT018C4	DH	5x5	3.00E+15
MT131A*	Hall	10x10	1.00E+15
MT139A*	Hall	10x10	1.00E+15
MT056A*	Hall	10x10	1.00E+15
MT176A*	Hall	10x10	1.00E+15
MT152A*	Hall	10x10	1.00E+15
MT082A*	Hall	8x8	1.00E+15
MT065A*	Hall	10x10	1.00E+15
MT131B*	DiffL	7x7	1.00E+15
MT139B*	DiffL	7x7	1.00E+15
MT027B*	DiffL	7x7	1.00E+15
MT176B*	DiffL	7x7	1.00E+15
MT152B*	DiffL	7x7	1.00E+15
MT082B*	DiffL	5x5	1.00E+15
MT065B*	DiffL	7x7	1.00E+15
MT018B*	DiffL	7x7	1.00E+15

* Irradiated but not reported here